JOM, Vol. 72, No. 12, 2020
https://doi.org/10.1007/s11837-020-04422-y

Support Thickness, Pitch, and Applied Bias Effects on the Carbide Formation, Surface Roughness, and Material Removal of Additively Manufactured 316 L Stainless Steel

ROBERT HOFFMAN,[1] SHAWN HINNEBUSCH,[2] SUBBARAO RAIKAR,[1] ALBERT C. TO,[2] and OWEN J. HILDRETH[1,3]

1.—Department of Mechanical Engineering, Colorado School of Mines, 1500 Illinois St, Golden, CO 80401, USA. 2.—Department of Mechanical Engineering and Materials Science, University of Pittsburgh, 4200 Fifth Ave, Pittsburgh, PA 15260, USA. 3.—e-mail: ohildreth@mines.edu

Advances in self-terminating etching processes have brought dissolvable supports to selective laser-melted stainless-steel alloys. Preliminary data showed that the amount of support material removed could be larger than the amount of material removed from the bulk material. This article details a small study aimed at understanding this phenomenon. First, the material removed and roughness as a function of applied bias is studied. From this, two different potentials were selected, 400 mV_{SHE}, which removes 120 μm through intergranular corrosion, and 550 mV_{SHE}, which removes material 39 μm through uniform corrosion. Next, a simulated set of support structures with wall thicknesses varying from 82 μm to 544 μm was etched under these two different potentials to report the range of thicknesses that can be reasonably removed.

INTRODUCTION

Post-processing metal components fabricated using laser powder bed fusion (L-PBF) additive manufacturing (AM) technologies present a significant challenge that both restricts design freedom and increases costs.[1] This is especially true for components with internal supports or internal features that are difficult to access using mechanical grinding methods traditionally used for AM component post-processing. To address this issue, the Hildreth group recently introduced a self-terminating etching technique that brings dissolvable supports to L-PBF metals.[2] This process, schematically illustrated in Fig. 1, begins by printing the components using existing equipment and printing parameters. Next, the component with attached supports and any trapped powder is immersed in an aqueous solution of saturated sodium hexacyanoferrate [$Na_4Fe(CN)_6{\cdot}10H_2O$] and allowed to dry, coating all surfaces with a layer of sodium hexacyanoferrate. The component is then put through the standard post-print heat treatment commonly used to remove residual stresses and refine the microstructure. The sodium hexacyanoferrate decomposes during this process to form a layer of surface carbon that then diffuses into the component's surface, where it captures the passivating chromium in chromium carbide precipitates. This reduction in free chromium "sensitizes" this region and reduces the corrosion potential, E_{corr}, below that of the stainless steel.[3] The sensitized component is then etched under conditions that keep the sensitized region under an anodic bias to dissolve the sensitized region while the underlying component material is kept at a protective cathodic bias to keep it from dissolving.[2] The net result is a geometry-agnostic, self-terminating etching process that removes a predefined amount of material from all surfaces—removing all the supports, trapped powder and surface defects. This process has been used to remove both external and internal supports while preserving the overall shape and tolerances. The 100–200 μm removed from the component should be compensated for with minor changes to the CAD model prior to fabrication.

(Received July 9, 2020; accepted September 26, 2020; published online October 26, 2020)

Internal studies have shown that supports can be considerably thicker than the component.[4] For example, conditions that remove 50 μm off the component's surface can be used to remove supports that are > 200 μm thick. To better understand this phenomenon, this work examines the difference in sensitized microstructure for supports with various thicknesses compared to bulk surfaces. Support thickness was varied from 82 μm to 524 μm by adjusting the number of laser passes and the pitch between the passes. Next, a small parameter space investigation was conducted to determine the impact of the applied bias on the amount of material removed and the resulting surface roughness. From this study, two biases were selected, 400 mV_{SHE} to test intergranular corrosion and 550 mV_{SHE} to test uniform corrosion, to etch sets of simulated support structures to compare how etching mechanisms impact the efficacy of support removal. These studies conclusively show that supports are more sensitive to carburization and that a broad range of applied biases can be used during electrochemical etching to remove the supports so that the process can be tailored to the needs of the component.

MATERIALS AND METHODS

Sample Preparation

An EOS M290 Direct Metal Laser Sintering (DMLS) system was used to print 316 L stainless steel supports of varying thicknesses and wall pitch printing parameters. The default printing parameters are the following: 100 W laser power, 675 mm/s scan speed and 40 μm layer thickness. Disc samples (15 mm diameter, 4 mm thick) for chronoamperometry tests were fabricated horizontal to the build platform. The disks were cut off the build platform using a wire electrical discharge machine (wire EDM). All electrochemical and etching studies were conducted on the top printed surface. Supports of different thicknesses were fabricated by varying the number of laser scan passes and the pitch between scans. The pitch was varied from 30 μm to 60 μm and the number of passes from one to seven passes to vary the wall thickness from 82 μm to 540 μm. Supplementary Fig. S-1 shows the layout of the support samples (refer to online supplementary material).

All chemicals were used as received from the supplier. The fabricated samples were rinsed with methanol (CH_3OH, ≥ 99.8%, Sigma Aldrich), acetone (CH_3COCH_3, ≥ 99.5%, VWR) and isopropanol (C_3H_8O, ≥ 99%, Pharmco), Excess fluid was removed from the surface by spraying it with gaseous nitrogen (N_2). A saturated solution of sodium ferrocyanide decahydrate ($Na_4Fe(CN)_6{\cdot}10H_2O$, ≥ 99%, Sigma Aldrich) was prepared, and the samples were submerged in the saturated sodium ferrocyanide decahydrate solution for 20 min to coat the surface. A slurry of sodium ferrocyanide decahydrate (SFCD) and deionized (DI) water (18.2 MΩ, Thermo Scientific Smart2-Pure) was prepared using a 4.2:1 mass ratio of SFCD to water and packed onto the samples. The samples were covered with graphite powder (C, < 20 μm, Sigma Aldrich) and wrapped in 309 stainless steel tool wrap (MSC Industrial Supply).

The samples were loaded into an inert gas furnace (DT-22-FL-VA-8, Deltech Furnaces) filled with argon gas (Ar) at room temperature (approximately 20–25°C) and heated to 50°C at a ramp rate of 5°C/min. The samples dwelled at this temperature for 1 h. This ramp and dwell cycles were repeated for temperatures of 90°C, 185°C and 250°C to allow any adsorbed water to evaporate and be evacuated from the furnace. This step is necessary to avoid the formation of a dense oxide layer that can inhibit etching. After the dwell cycle at 250°C, the samples were heated to 800°C at a ramp rate of 5°C/min and were held at this temperature for 6 h. The furnace was then cooled to 30°C by cooling the temperature of the furnace by 5°C/min. The samples were then unloaded from the furnace and the stainless-steel foil was removed. Carbon agglomerated on the

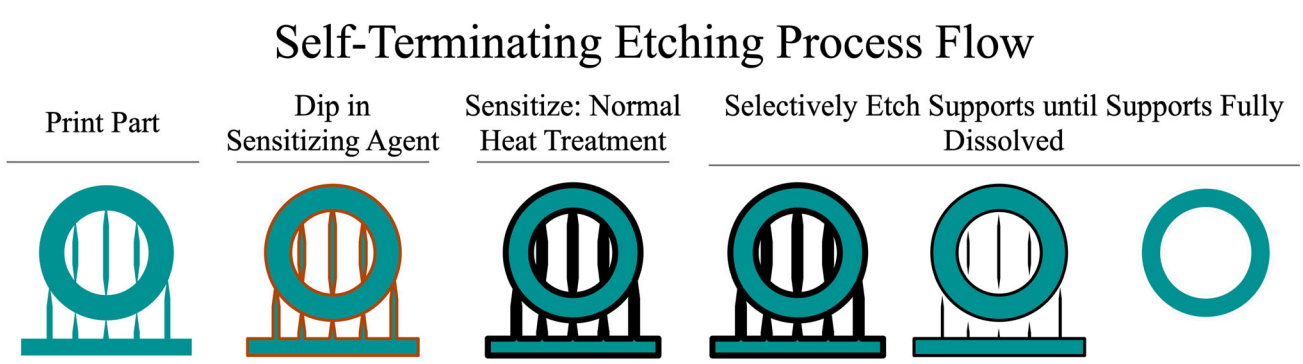

Fig. 1. Schematic of the self-terminating etching process. L-PBF components are first printed using existing equipment and printing parameters. Next, the sample is dipped in sodium hexacyanoferrate to coat all surfaces in this sensitizing agent. During heat treatment, the sodium hexacyanoferrate decomposes to form a layer of carbon that diffuses into the component and captures the chromium to form a sensitized region at the surface, including all of the supports. This sensitized region can then be selectively dissolved to remove the supports and surface defects.

sample during the heat treatment was removed from the sample using a stainless-steel bristle brush, then cleaned in an ultrasonic water bath for 5 min and rinsed in DI water. The dirty water in the sonicating bath was also replaced with clean water at this time. The sonication cycle was repeated until the ultrasonic bathwater remained clear of contaminants, suggesting that most of the heat treatment byproducts were removed from the surface of the sample. The samples were rinsed with methanol, acetone and isopropanol. Excess fluids were removed from the surface by spraying the surface with nitrogen gas (N_2).

Electrochemistry and Metrology

Electrochemical experiments were conducted using a Princeton Applied Research PARSTAT MC 1000 chassis equipped with eight PMC 1000 potentiostat cords. A jacketed corrosion cell (Pine Research, OpenTop Cell with Water Jacket and Drain Valve) was filled with a mixture of 0.48 M nitric acid (HNO_3, 70 wt.%, VWR Chemicals) and 0.1 M potassium chloride (KCl, 99 wt.%, Macron Chemicals). The corrosion cell was set up with a salt bridge containing 4.0 M potassium chloride solution, a silver/silver chloride (Ag/AgCl) electrode in 4.0 M KCl and a 6.35-mm-diameter graphite counter electrode. Prior to use, all reference electrodes were checked against the laboratory's "master" Ag/AgCl reference electrode, with typical shifts on the order of 1–2 mV. All electrochemical measurements were shifted by and assumed − 197 mV and were reported relative to the standard hydrogen electrode (SHE).

The open circuit potential (OCP) was measured for 5 min for as-printed and sensitized samples. Cyclovoltammetry (CV) was collected ± 100 mV about the OCP at 10 mV/s. Chronoamperometry (CA) for 15 h at constant potential was collected on sensitized disk samples to determine the amount of material removed and resulting surface roughness as a function of applied bias. All disc samples were held in a custom holder that exposed 12.5 mm^2 of printed side disks to the electrolyte. The two support grid samples were wrapped in stainless steel wire and the corrosion cell and were used as the working electrode. The potentiostat was used to first measure the sample's open circuit potential for 5 min, then cyclic voltammetry curves for three cycles ± 100 mV about OCP and chronoamperometry at a voltage of either 400 mV_{SHE} or 550 mV_{SHE} for 24 h (which is more than enough time to remove the support structures).

Surface roughness and the remaining support profiles were measured using a contact profilometer (Bruker, DektakXT) equipped with at 2-μm stylist at 3 μg force with 90 s scans of 5 mm length. The remaining support width and heights were recorded by measuring the profile thickness and height. Remaining support thicknesses were measured by modifying the profilometer cursor width to match the profile width, while support heights were measured using the difference in cursor heights.

Mounting, Cutting and Polishing

The sensitized individual support samples were sectioned along the length of the support samples using a precision saw with a diamond CBN blade (Buehler, Isomet Low Speed Saw). The samples were then hot mounted using approximately 10 ml copper (Allied High-tech) and 15 ml Bakelite. The sensitized support grid was sectioned using an MSX-250 saw with an aluminum oxide (Al_2O_3) abrasive blade. The samples were then mounted in epoxy (Epofix, Struers) and sectioned again using the MSX saw. The samples were ground using 180, 320, 400 and 600 grit silicon carbide paper (Leco) and then polished using 6 μm and 1 μm diamond suspensions (Leco).

For carbide reveal, the polished samples were submerged in a solution of 1.11 M oxalic acid (HO_2CCO_2H, 98%, Sigma Aldrich), and a potential of 6.0 V was applied across the samples using stainless steel and copper as the electrodes for 30 s. The samples were placed into an ultra-sonic DI water bath for 5 min. The samples were removed from the water bath and rinsed in ethanol. The samples were sprayed with gaseous N_2 to remove excess fluid from the surface. The microstructure of the samples was imaged using a Zeiss Axio Vert. A1 while other images were taken with a Nikon D7000 camera. The region thicknesses were measured using the image processing software ImageJ.

RESULTS AND DISCUSSION

Carbon is a known sensitizing agent for stainless steels.[3,5–12] At high temperatures, surface carbon diffuses into the component and captures the chromium in chromium carbide precipitates forming intergranular carbides initially along the grain boundaries and then forming intragranular carbides as the carbon concentration increases.[5–8] These carbides effectively decrease the concentration of "free" chromium, and, once the concentration decreases to below ~ 12 wt.%, the "sensitized" region is no longer able to form a self-passivating oxide.[3,9] The potentiodynamic polarization plot in Fig. 2a illustrates this effect. The corrosion potential (E_{corr}) of the as-printed, unsensitized 316 L sample is ~ 555 mV_{SHE} with extremely low current densities on the order of $\mu A/cm^2$ while the corrosion potential for the sensitized sample drops by ~ 600 mV to − 55 mV_{SHE}. As a result, any potential > − 55 mV_{SHE} will cathodically dissolve the sensitized region while any potential below 555 mV_{SHE} will anodically protect the underlying unsensitized bulk. This difference in corrosion response is what enables the self-terminating etching process we use to selectively remove support structures from L-PBF metal components.

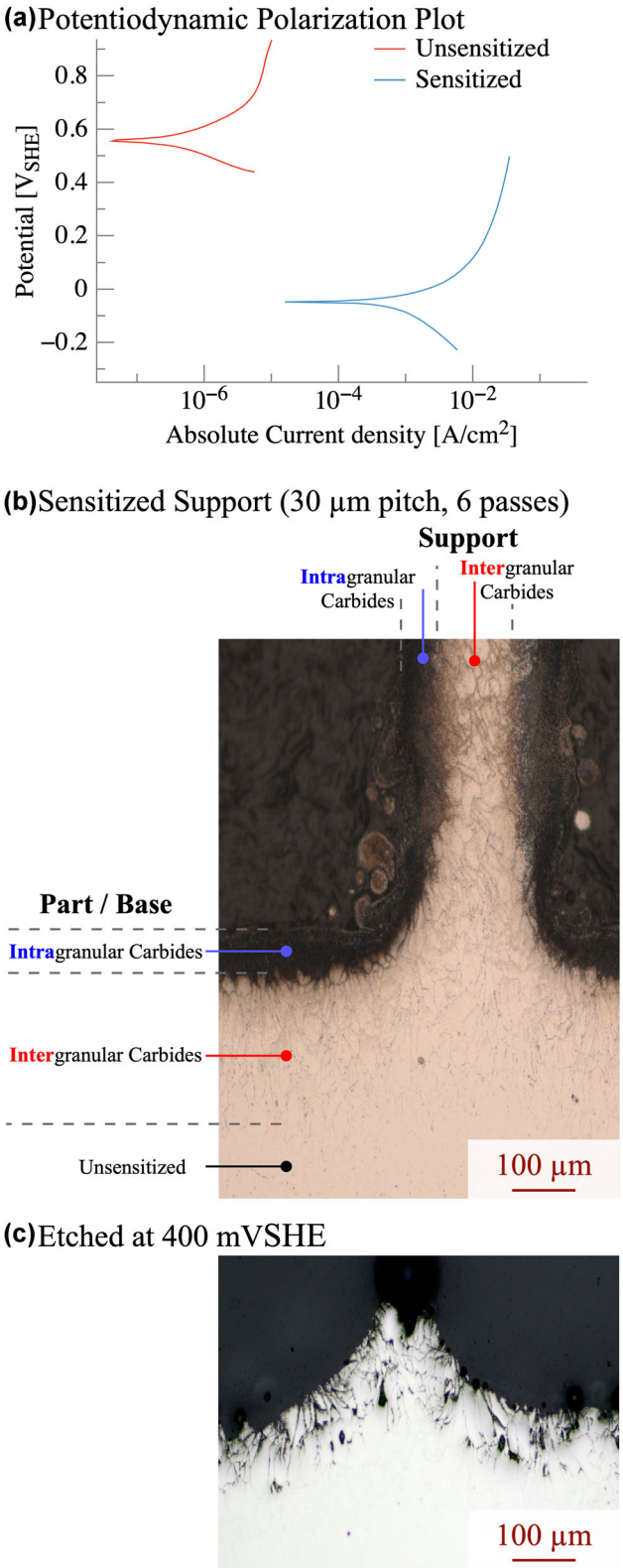

◀Fig. 2. (a) Potentiodynamic polarization plot of the as-printed sample (blue) and the sensitized sample (red).[13] Sensitization drops E_{corr} by 600 mV, opening up a wide processing window where the sensitized region can be dissolved while the underlying component is cathodically protected. (b) Sensitized support showing the intragranular carbides and intergranular carbides for the support and the part. (c) Cross-section after etching at 400 mV_{SHE}; notice that the supports are removed, but significant intergranular corrosion is observed at this potential (Color figure online).

As shown in Fig. 2b, both intragranular and intergranular carbides form within the supports and the surface of the component. Figure 2c shows the remnants of this particular support structure after etching at 400 mV_{SHE}. The width of intragranular carbide and intergranular carbide regions directly impacts the amount of material that can be removed at a given bias.[4] In general, regions with larger amounts of intragranular carbides are more sensitized, have a lower E_{corr}, do not form strong passivation layers and can be removed across a wider range of potentials.[10] The intergranular carbide regions, while still sensitized, can still form passivation layers at sufficiently high potentials. As shown in Fig. 3, these differences can be exploited to select biases that activate different corrosion mechanisms with resulting differences in the amount of material removed and surface roughness.

The graphs in Fig. 3 plot the amount of material removed and total profile roughness versus the applied bias as measured on the sensitized 316L disks. The red and blue markers were used to highlight the results for the 400 mV_{SHE} (red triangle) and 550 mV_{SHE} (blue square) potentials used to etch the support thickness samples used to study how support thicknesses and scan strategies impact support removal. A 400 mV_{SHE} bias was selected because it removed the most material (120 μm) while still providing reasonable roughness (R_a^{mean} = 7 μm). The 550 mV_{SHE} was selected because it provides the smoothest surface (R_a^{mean} = 6 μm, R_a^{min} = 2.9 μm). While 200 mV_{SHE} was considered because of its similarity to 550 mV_{SHE}, the top-down SEM images revealed 550 mV_{SHE} provided a more uniform coating of chromium oxide particles, whereas the 200 mV_{SHE} sample had visible voids on the sample surface leading to a less protective oxide layer compared to the 550 mV_{SHE} sample. The top-down SEM images can be seen in supplementary Fig. S-2.

Supplementary Fig. S-1 shows the layout of the test samples simulating supports of different widths. Support width was varied by adjusting the number of laser scans and the pitch between these scans with seven walls made per setting connected

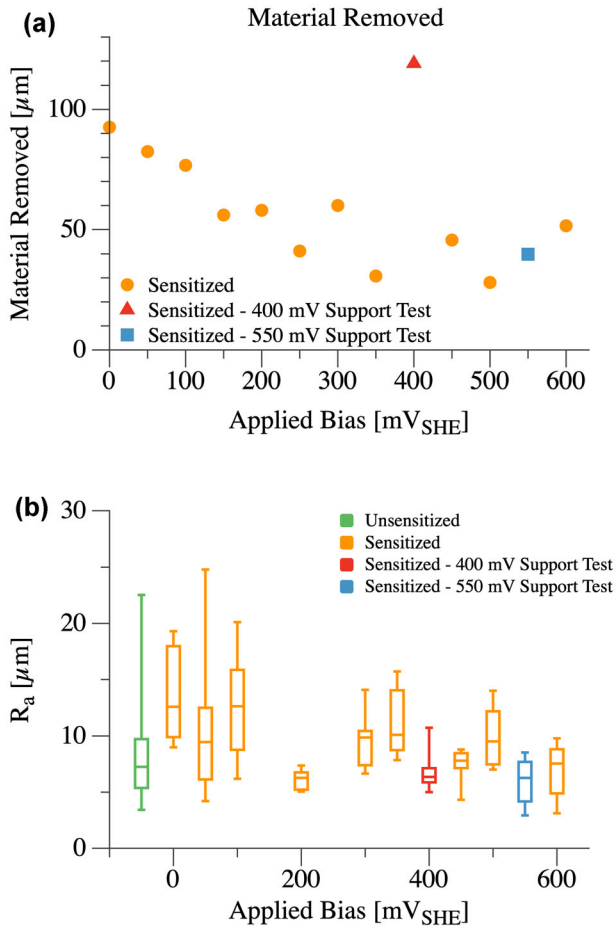

Fig. 3. Graphs showing the measured material removed (a) and R_a surface roughness (b) from CA tests on disc samples. Green shows the results for the unsensitized samples while orange, red and blue are for the sensitized samples. Red (400 mV_{SHE}) and blue (550 mV_{SHE} highlight the potentials used on the support wall thickness samples. The reported surface roughness is the total profile roughness of the part. Notice that 400 mV_{SHE} removed the most material while 550 mV_{SHE} created the smoothest surface (Color figure online).

with an outer skin to ensure structural integrity and better mimic the diffusion-limited conditions that can form during etching. In supplementary Fig. S-1a, each row corresponds to a different pitch between 30 μm and 60 μm and each column shows a different number of passes (note that the 50 μm row starts at one laser scan instead of two scans as in the other rows). The numbers below each set show the expected support width. Supplementary Fig. S-1a plots the measured support thickness (from cross-sections) versus the expected width. Overall, there is a good correlation between the measured and expected widths with the measured widths as seen by the mostly linear fit in Fig. S-1b.

Figure 4 shows the samples before sensitization (column a) and then after etching at 400 mV_{SHE} (column b) and 550 mV_{SHE} (column c). The top row shows top-down images, and the second row shows a side view to illustrate the ability of the process to remove a wide range of support widths. The third and fourth rows show cross-section images stained to reveal carbides. For these samples, the as printed, unsensitized surface had sections that were relatively smooth, but still had a large range in R_a values (see Fig. 3b). Etching at 400 mV_{SHE} reduced the range in R_a values, but the bias is too low to form a passivating layer at the sensitized grain boundaries in the intergranular carbide region, and deep intergranular corrosion is observed even though the surface is capped by a relatively smooth region of intragranular corrosion. The 550 mV_{SHE} is closer to the potential that can passivate the regions sensitized [4] with intergranular carbides, and a deep intergranular corrosion region is not observed. However, 550 mV_{SHE} is still slightly off the ideal bias for this sample because some surface corrosion is observed, and the average roughness is still higher than the 2.4 μm R_a roughness achieved previously.[4]

For a bulk component, the mean thickness of the intragranular carbide region is 40 μm followed by 120 μm of intergranular carbides. Figure 5a and b graphs the thickness of the (a) intragranular carbide region and (b) total carbide region as a function of the measured width. The dashed line shows the 1/2 support width calculated from supplementary Fig. S-1b. Data above this line indicate that the support was fully sensitized, and data below this line indicate partial sensitization. The purple line shows the thickness of (a) intragranular and (b) total carbide regions in the bulk component. These data are normalized using the measured support thickness in Fig. 5c and d. Notice that the thickness of the intragranular region in the supports is significantly higher than that of the bulk component. This is likely because the scan strategies for support structures are different from those used in bulk. Support structures are often scanned at higher speeds with an emphasis on throughput while density may not be as crucial. In contrast, scan strategies for bulk components are heavily optimized for improved density and low porosity. As a result, supports are sensitized to a much higher degree than the bulk component. This opens up the possibility that sensitization heat treatment schedules could be optimized to use lower temperatures or times and still achieve the required sensitized depths for full support removal.

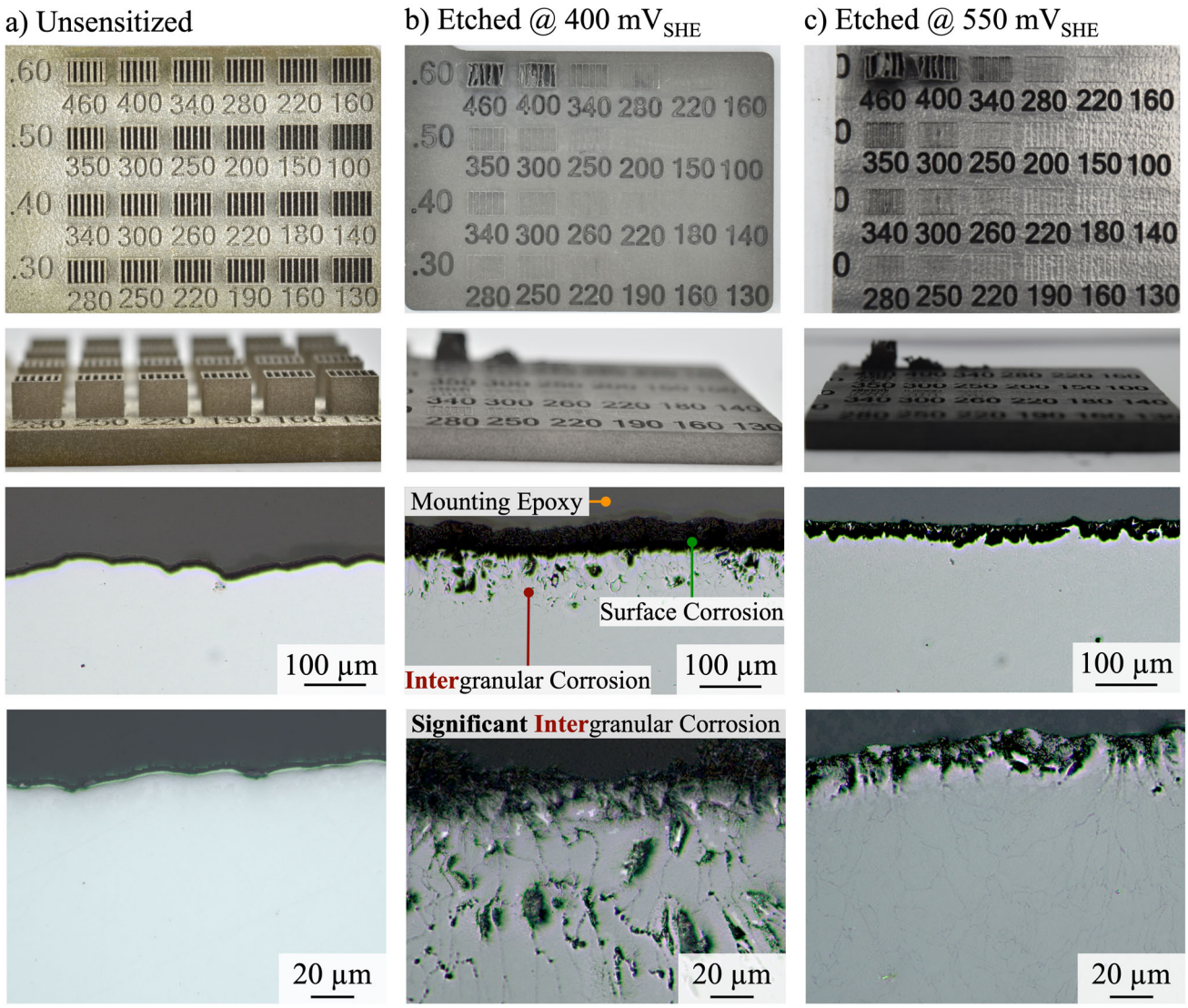

Fig. 4. Optical camera and microscope images showing the results of the support thickness experiments. (a) The original as-printed/unsensitized supports; (b) after etching at 400 mV$_{SHE}$; (c) after etching at 550 mV$_{SHE}$. Notice that the 400 mV$_{SHE}$ sample results in $\sim$ 100 μm of intergranular corrosion while the 550 mV$_{SHE}$ sample has $\sim$ 20 μm of surface corrosion.

The quantified support grid etch results in Fig. 6 and 7 further support our claim that the amount of support structure removed can be significantly larger than the amount of material removed from the bulk of the sample. The graphs in Fig. 6 show the amount of height and width remaining for the support structures etched at 400 mV$_{SHE}$ 550 mV$_{SHE}$. A dashed line was added at two times the amount of material removed from the bulk samples (as measured on the disc samples) to highlight that even though only 40 μm is removed from the bulk sample at 550 mV$_{SHE}$, $<$ 100 μm of support material is left behind for supports $<$ 300 μm wide. Additionally, notice that the remaining support material height is generally less for the 550 mV$_{SHE}$ samples compared to those etched at 400 mV$_{SHE}$; however, only the 400 mV$_{SHE}$ bias was able to essentially remove the supports completely (remaining height $\leq$ 1 μm for the samples with 30 μm and 50 μm and support widths $<$ 130 μm. Figure 7 normalized the data from Fig. 6 by graphing the remaining height versus the percentage of the supports that contained intragranular carbides (a and b) and any carbides (c and d). The data in Fig. 7 show that certain scan pitches (30 μm and 50 μm) resulted in high degrees of intragranular carbides and left behind smaller amounts of support material. This finding alongside the data presented in

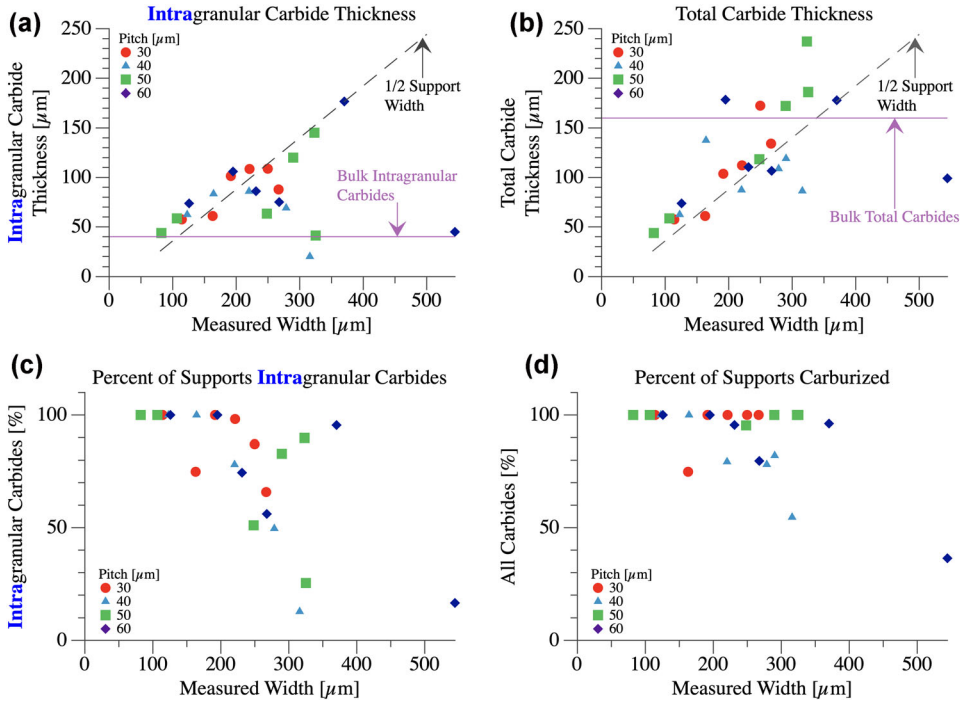

Fig. 5. Graphs showing the relationship between measure width of the supports and the percentage of the support with intragranular carbides (a, c) and any carbides (b, d). The dashed line shows the 1/2 support width calculated from supplementary Fig. S-1. The purple line shows the thickness of (a) intragranular and (b) total carbide regions in the bulk component. Notice that supports < 200 μm wide are fully sensitized with intragranular carbides, and most supports are fully carburized once both intragranular and intergranular carbides are included. Additionally, the 40 μm pitches are harder to fully sensitize, indicating that scan-induced microstructure differences could impact sensitization.

Figs. 5 and 6 indicates that supports with higher amounts of intragranular carbides are easier to remove and they leave behind fewer residual supports post etching.

CONCLUSION

Overall, this work provides some interesting insights into the differences between removing support structures and removing the surface material from a bulk component. This demonstrates that the degree of sensitization, as revealed by intragranular and total carbide depth, is significantly higher in support structures compared to bulk components, resulting in a high sensitization depth for the supports even if the bulk is only minimally sensitized. Since this sensitization depth varied significantly with scan strategy, we speculate that this difference in sensitization between the support structures and the bulk components is due to increased porosity within the support structures allowing for better surface reactions during carburization. The other possible cause is differences in microstructural development with phase formation and grain structure during the heat treatment process, which impacts the chromium precipitation during carburization of the part. These hypotheses will be tested in future work.

Scan strategies that optimize intragranular carburization should be used when printing parts. Scan pitches between 30 μm and 50 μm are preferred. Support thickness also needs to be considered when printing parts. Researchers and engineers should consider using supports ≤ 200 μm in thickness to efficiently remove supports with one sensitization cycle.

This work conclusively shows that extremely thick support structures (such as the support structures seen in the works of Lefky cited in this

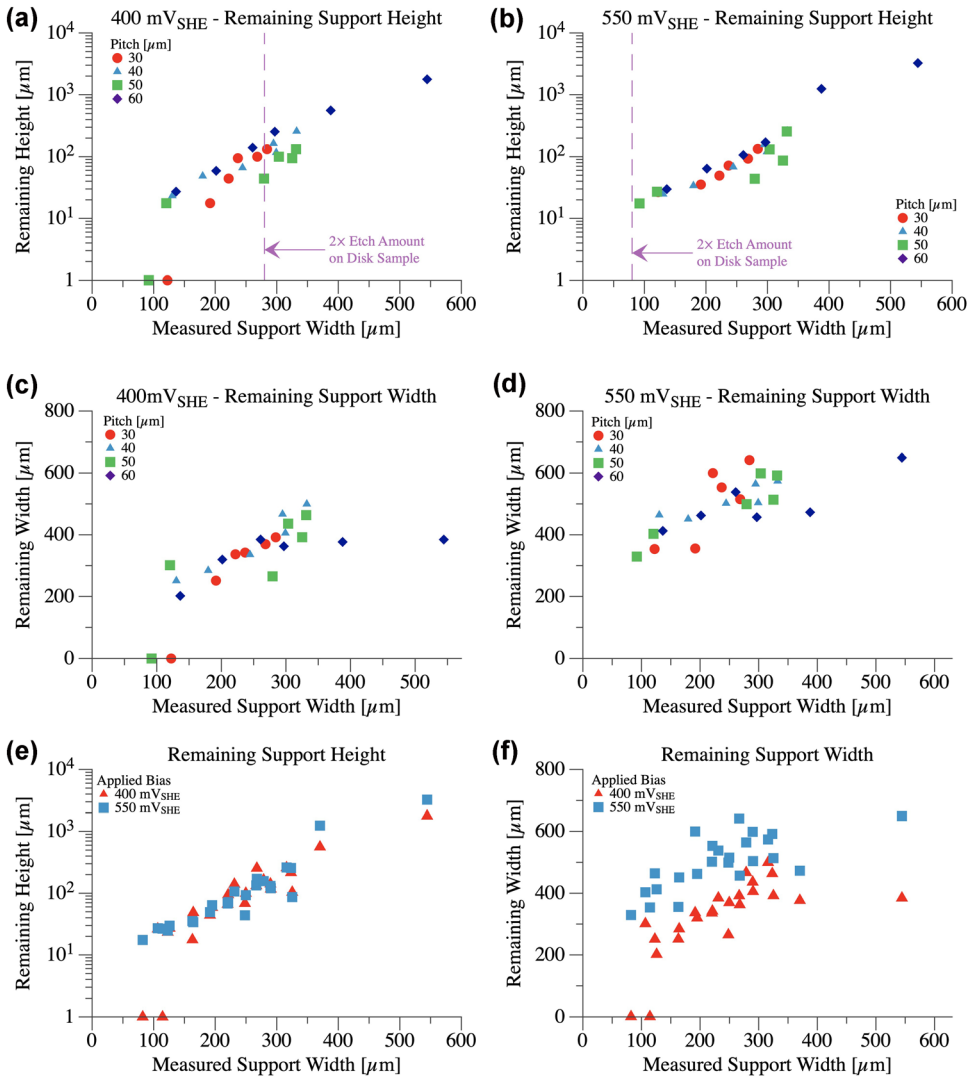

Fig. 6. Graphs showing the amount of remaining support height and width as a function of applied potential when etched at 400 mV$_{SHE}$ (a, c) and 550 mV$_{SHE}$ (b, d). The data for the remaining height (a, b) and the remaining width (e, f) were consolidated into one graph for a better comparison of the two data sets. The dashed purple line indicates two times the amount of material removed from the bulk sample at the respective potentials. Notice that the 550 mV$_{SHE}$ sample removed slightly more height from the supports even though the smaller remaining support is slightly wider.

manuscript) can be removed under biases that result in an improved surface roughness if sufficient carburization occurs during sensitization. This has important implications for optimizing this process for surface roughness. To produce a smooth surface even if the support structures are relatively thick, researchers and engineers will not need to increase sensitization times and temperatures or use biases that aggressively attack sensitized grain boundaries (400 mV). They can use biases that optimize the overall part surface roughness (550 mV) to achieve similar results. Typically, end users prefer to use biases that optimize surface roughness so 550 mV would be a more desirable bias for industrial use.

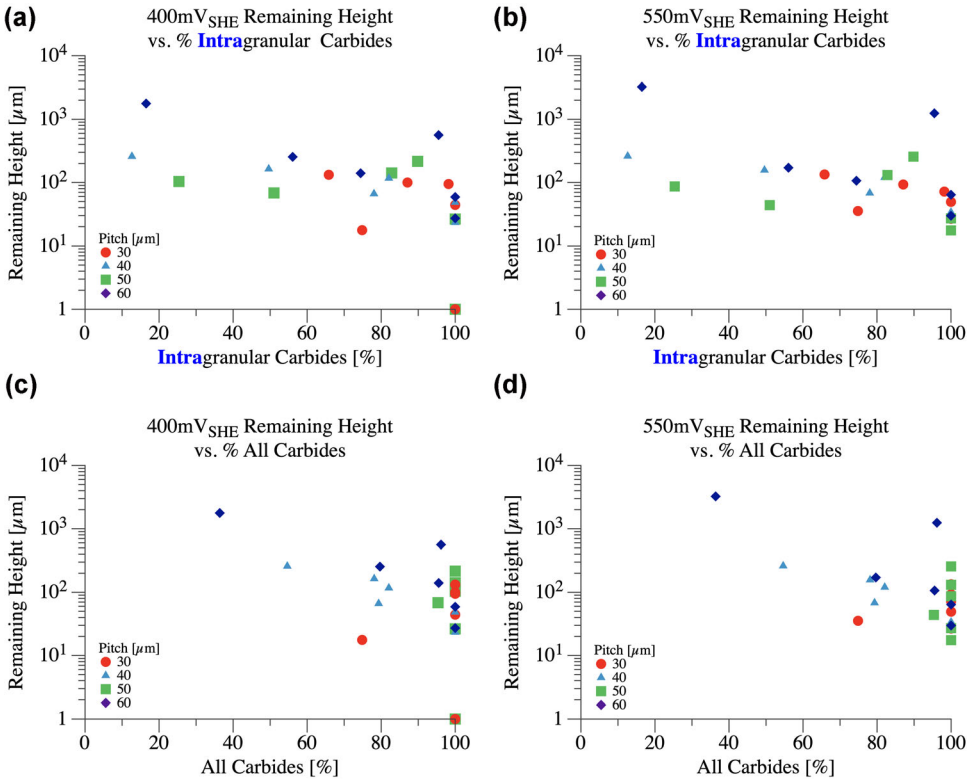

Fig. 7. Graphs showing the remaining support height versus (a, b) the percentage of the supports with intragranular carbides and (c, d) the percentage of the supports with any carbides.

ACKNOWLEDGEMENTS

Hildreth group gratefully acknowledges the support from the Department of Energy, Nuclear Energy University Program (NEUP Project 18-15251), the National Science Foundation (CAREER 1944516) and the Colorado Office of Economic Development and International Trade (CTGG1 20-2072). To Group (A.C.T. and S.H.) gratefully acknowledges the support from the Department of Energy, Nuclear Energy University Program (NEUP Project 18-15251). Any opinions, findings and conclusions or recommendations expressed in this material are those of the author(s) and do not necessarily reflect those of the Department of Energy, the National Science Foundation or the Colorado Office of Economic Development and International Trade.

CONFLICT OF INTEREST

The authors declare that they have no conflict of interest.

ELECTRONIC SUPPLEMENTARY MATERIAL

The online version of this article (https://doi.org/10.1007/s11837-020-04422-y) contains supplementary material, which is available to authorized users.

REFERENCES

1. Wohlers Associates, *3D Printing and Additive Manufacturing State of the Industry*, Vol. 23 (Fort Collins: Wohler Associates Inc., 2018), p. 344.
2. C.S. Lefky, T.G. Gallmeyer, S. Moorthy, A. Stebner, and O. Hildreth, *Addit. Manuf.* 27, 526 (2019).
3. N. Parvathavarthini and U.K. Mudali, *Corros. Rev.* 32, 183 (2014).
4. C.S. Lefky, Corrosion and Sensitized Microstructure Evolution of 3D Printed Stainless Steel 316 and Inconel 718 Dissolvable Supports, Doctoral Dissertation, Arizona State University (2018).
5. F.B. Litton and A.E. Morris, *J. Less-Common Met.* 22, 71 (1970).
6. G.G. Tibbetts, *Appl. Phys.* 51, 4813 (1980).
7. G. Millward, H. Evans, M. Aindow, and C. Mowforth, *Oxid. Met.* 56, 231 (2001).

8. T. Turpin, J. Dulcy, and M. Gantois, *Metall. Matter. Trans. A* 36, 2751 (2005).
9. H.J. Grabke, R. Krajak, and J.C. Nava Paz, *Corros. Sci.* 35, 1141 (1993).
10. P.O. Atanda, A. Fatudimu, and O. Oluwole, *J. Miner. Mater. Charact. Eng.* 9, 13 (2010).
11. D. Farkas and J. Delgado, *Scr. Metall.* 17, 261 (1983).
12. S.K. Balijepalli, L. Ceschini, C. Chiavari, S. Kaciulis, C. Martini, A. Mezzi, R. Montanari, and G. Verona Rinati, *Surf. Interface Anal.* 46, 731 (2014).
13. C.S. Lefky, B. Zucker, D. Wright, A.R. Nassar, T.W. Simpson, and O.J. Hildreth, *3D Print Addit. Manuf.* 4, 3 (2017).